Zeitschrift für anorganische und allgemeine Chemie

Journal of Inorganic and General Chemistry
ZAAC
Zeitschrift für anorganische und allgemeine Chemie

RESEARCH ARTICLE OPEN ACCESS

Jet Mixer Precipitation vs. Conventional Precipitation for a Cu/ZnO/MgO MeOH Catalysts

Lukas D. Ernst[1,2] | David Guse[3] | Noah Schmidt-Meinzer[1,2] | Matthias Kind[3] | Ingo Krossing[1,2]

[1]Institut für Anorganische und Analytische Chemie, University of Freiburg, Freiburg, Germany | [2]Freiburger Materialforschungszentrum (FMF), University of Freiburg, Freiburg, Germany | [3]Institute of Thermal Process Engineering (TVT), Karlsruhe Institute of Technology (KIT), Karlsruhe, Germany

Correspondence: Ingo Krossing (krossing@uni-freiburg.de)

Received: 18 November 2025 | **Revised:** 26 January 2026 | **Accepted:** 19 February 2026

Keywords: catalyst synthesis | co-precipitation | heterogenous catalysis | methanol synthesis | oxidative fluorination

ABSTRACT

The synthesis of precursors for MeOH catalysts usually takes place *via* coprecipitation, where a metal solution is precipitated with a precipitant and aged in a temperature-controlled reactor. Due to the limited addition rate of the solutions, in many cases precipitation overlaps with aging and particles are still being precipitated while the first particles are already aging. In order to better separate precipitation and aging, a jet mixer apparatus enabling this task was developed at the Institute of Thermal Process Engineering (TVT) of KIT. In this work, a Cu/ZnO/MgO catalyst system was produced using both conventional coprecipitation and jet mixer precipitation. Both systems were then exposed to gaseous difluorine to improve the catalyst properties by oxidative fluorination. A comparison of both catalyst classes produced this way showed that the properties of the systems precipitated conventionally or with the jet mixer to be comparable (metal content, surface area, infrared spectra, powder diffractograms). However, two significant differences were observed: the additional presence of an aurichalcite phase in the conventionally produced system and a significantly higher particle size of secondary particles in the jet mixer system. In terms of catalytic performance, the differences are small and the system prepared by jet mixer showed slight superiority with a by 7% higher MeOH synthesis rate under standard measurement conditions for the nonfluorinated system as well as 1–7 kJ mol^{-1} lower apparent activation energies for MeOH formation.

1 | Introduction

The precipitation synthesis route to Cu/Zn-based catalysts for CO_2 hydrogenation to methanol [1–21] is an essential step that significantly determines the properties of the subsequent catalyst system. Typically, the precipitation synthesis is carried out as coprecipitation [22], with basically three variants: (i) forward coprecipitation: the solution of the metal salts is presented and the precipitating agent is added, (ii) reverse coprecipitation: the precipitating agent is presented and the solution of the metal salts is added, and (iii) continuous coprecipitation, in which both solutions are added simultaneously. Due to the significantly different pH development between the Cu/Zn-based coprecipitations according to protocol (i) to (iii), the resulting precipitates differ greatly among the three variants. The typically preferred Cu/Zn-based precipitation variant is continuous coprecipitation, which produces less complex product mixtures. Often, precipitation is followed by an aging period during which the amorphous precipitation product, Zincian Georgeite, transforms into the crystalline Zincian Malachite (a process known as mesostructuring). This transformation is accompanied by a color change from blue (precipitation product) to green (aged precipitate) [23, 24]. During continuous coprecipitation, the synthesis takes place in a batch reactor, and the solutions are usually added via controlled pumps over a set time period. For instance, the solutions used in the syntheses performed in this study were added at 13 mL min^{-1} over a total of 40 min. However, precipitation and aging occur on different timescales. While precipitation occurs in milliseconds to

seconds, aging usually takes 30 min to several hours [25, 26]. Therefore, in conventional coprecipitation, the processes of precipitation and aging overlap. Particles that have just been precipitated coexist with particles that were precipitated earlier and are already in the aging process. Hence, it is not possible to clearly separate aging from precipitation.

To avoid this problem, at the institute of thermal process engineering (TVT) a specialized experimental setup was developed. At the heart of this apparatus is a jet mixer, which is a Y-piece that mixes the metal nitrate solution with the precipitant solution at a high pumping speed (here: 250 mL min^{-1}). The mixture is fed into a reactor where the actual aging step takes place (see Figure 1).

To investigate whether a Cu/ZnO/MgO (CZMg) catalyst system prepared by continuous coprecipitation gains from being produced with the jet mixer technique of TVT and to study its catalytic properties, a precipitation synthesis of the CZMg system was performed at TVT (=> CZMg_TVT) using parameters closely aligned with the conventional synthesis at FMF (=> CZMg_FMF). We compare the physicochemical properties and catalysis results of CZMg_TVT and _FMF, the latter of which has already been published [27]. Treatment of the CZMg system with elemental difluorine [27]—an oxidative fluorination [28–31]—improves the catalytic properties, particularly the long-term stability. This (fluorinated) CZMg system was shown to be capable of dealing with pure CO_2/3 H_2 streams, which is problematic for many commercial systems optimized for CO-rich $CO/CO_2/H_2$ streams. The stoichiometrically formed water present after reaction with a pure CO_2/3 H_2 stream deactivates the catalyst systems, e.g., with Al_2O_3 as support oxide. A known CO_2-tolerant alternative uses the more expensive ZrO_2 as support oxide (=CZZ). In this context, the fluorinated CZMg system was shown to be equal to CZZ at much lower cost. Hence, in this work, the CZMg_TVT system was precipitated using the jet mixer, and the calcined precatalyst was subjected to oxidative fluorination.

2 | Results and Discussion

At the Freiburg Materials Research Center (FMF), coprecipitation is typically performed using a metal nitrate solution with a cumulative metal concentration of 1.0 m and metal ratios of Cu:Zn:Mg = 3.75:1.74:1.00, along with a 1.5 m Na_2CO_3 solution [29, 31, 32]. Both solutions are added through continuous coprecipitation at 70°C. Initially, 0.5 L of tempered water is placed in the reactor, and then, more tempered water is added continuously to a total of 2.8 L (for pumping speeds see Supporting Information (SI) section 2.1). The precipitation reaction proceeds over 40 min, during which the addition rate of the Na_2CO_3 solution is controlled to maintain a pH of 7.0 ± 0.1. This is followed by a 1-hour aging period for the CZMg system, during which the pH value is not controlled. The CZMg system's crystallization onset is characterized by a pH drop during the aging period (Figure 2, top).

This precipitation procedure for the CZMg system has now been adapted to be carried out in the jet mixer apparatus of TVT [26]. The jet mixer enables for a comparable amount of liquids a precipitation time of around 4 min. Therefore, the aging time was adjusted so that the characteristic drop in the pH value was observed (Figure 2, bottom). Yet, the concentration of the metal nitrate solution had to be reduced to 0.5 m (1.5 L). Otherwise, the suspension of precipitation products in the jet mixer would have been too viscous to be pumped any further. Similar to the FMF precipitation, 0.5 L of tempered water was initially placed in the TVT reactor, but no additional tempered water was added during the process. Unlike in the FMF coprecipitation, the metal nitrate solution with reduced concentration (1.5 L, 0.5 m) and the sodium carbonate solution (2 L, 0.5 m) were heated to 70°C. Overall, in the moment of precipitation, therefore, in both setups the concentrations were rather similar. Only the process time for mixing the feed streams — 4 min with TVT Y-mixer vs. 40 min in the conventional FMF setup — differs by a factor of 10. Accordingly, the time-dependent pH- and temperature-curves of

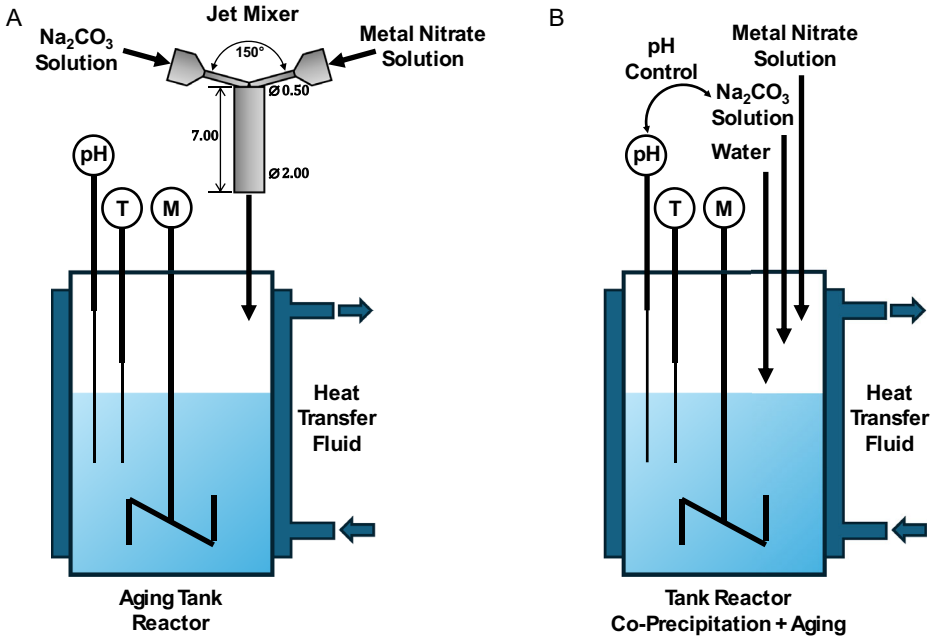

FIGURE 1 | (A) Schematic overview of the apparatus developed at TVT for separating precipitation and aging. (B) Schematic overview of the reactor for co-precipitation synthesis used for the FMF systems. Figure created according to Guse et al. [26].

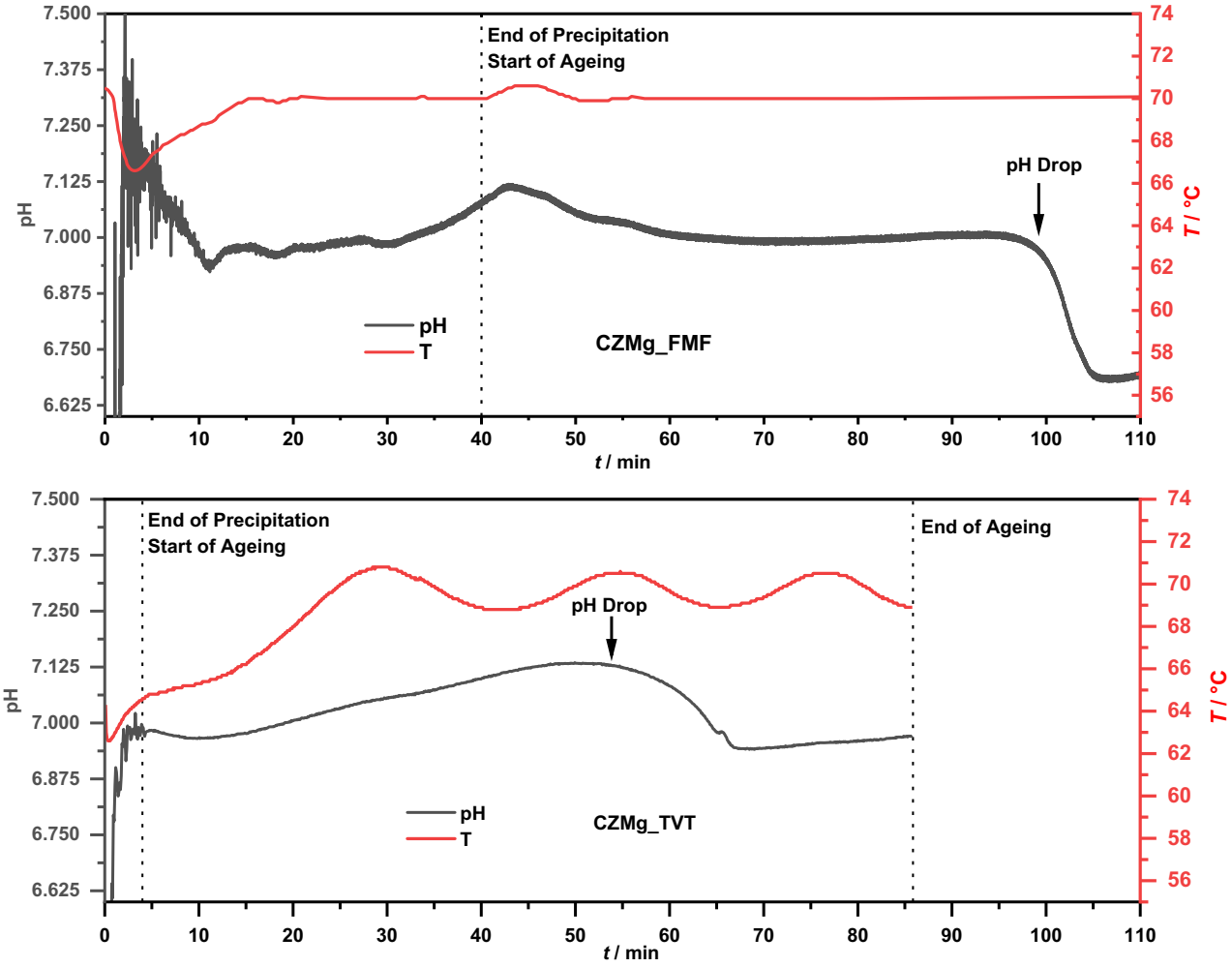

FIGURE 2 | Top: Temperature and pH profile in the stirred tank reactor during the precipitation period (0–40 min) and the aging period (40–100 min), FMF synthesis method. Bottom: Temperature and pH profile in the aging tank following the continuous precipitation in the Y-mixer (0–4 min), TVT synthesis method.

FMF and TVT coprecipitations shown in Figure 2 correspond well to each other. The TVT coprecipitate was filtered, washed with water to a conductivity below 500 μS cm^{-1}, and dried overnight in a vacuum drying oven at 40°C. The obtained TVT precursor was transferred to FMF, ground as finely as possible using an agate mortar, calcined in the FMF set up, and subsequently treated identical to the catalyst systems produced at the FMF. Both, CZMg_TVT or CZMg_FMF systems were oxidatively fluorinated to three degrees of fluorination, where the ending _FXXXX gives the cumulated applied fluorine pressure per 1.5 g of precatalyst in mbar (i.e., _F200, _F1250 and _F2500). Fluorination was done according to our optimized procedure reported earlier [27], cf. SI of this work. In the following, the pristine and fluorinated FMF and TVT CZMg catalyst systems are compared.

2.1 | Overview of the Standard Analysis of TVT Systems

The investigation of the TVT precursor (filtered, washed, and dried precipitate), the pristine precatalyst (calcined precursor), and the fluorinated precatalysts using powder X-ray diffraction (pXRD), IR spectroscopy, thermal gravimetric analysis (TGA) and surface area, pore volume and diameter determination using N_2 physisorption according to Brunauer, Emmett, and Teller (BET) gave results typical for the pristine and fluorinated CZMg precursor and precatalysts. The individual results for the CZMg_TVT system are compared with those published [27] for CZMg_FMF material in the next sections. Table 1 gives an overview about compositions, BET areas, and pore sizes of both series of samples.

2.2 | Comparison of Standard Analytical Data for the FMF and TVT Systems

The typical three steps to precatalyst synthesis (precipitation synthesis, calcination, and subsequent fluorination) were investigated with standard analytical methods, and the TVT and FMF [27] systems are compared for each of these three steps in the following.

2.2.1 | Precipitation and Calcination

2.2.1.1 | Precursors. The pXRD traces of the TVT precursor and the FMF precursor show a very similar picture; the mixed

TABLE 1 | Overview to compositions,[a] BET areas, and pore sizes of the pristine and fluorinated CZMg_TVT as well as published values of [27] CZMg_FMF precursor and precatalysts.

Precursor or calcined Precatalyst	Theoretical F^- content fluorinated precatalyst[b]/wt%	IC F^- content fluorinated precatalyst/wt%	SA_{BET} precatalyst/ $m^2\ g^{-1}$	Total Pore Volume/$cm^3\ g^{-1}$	Median d_{pore}/nm
CZMg_TVT_precursor	—	—	144	0.382	10.6
CZMg_TVT	—	—	121	0.492	16.3
CZMg_TVT_F200	1.4	1.2 ± 0.1	127	0.516	16.3
CZMg_TVT_F1250	8.4	8.5 ± 0.4	102	0.466	18.3
CZMg_TVT_F2500	16.2	12.4 ± 0.6	96	0.446	18.5
CZMg_FMF_precursor	—	—	124	0.465	15.0
CZMg_FMF	—	—	121	0.709	23.5
CZMg_FMF_F200	1.4	1.4 ± 0.1	103	0.613	23.9
CZMg_FMF_F1250	8.4	7.4 ± 0.3	82	0.517	25.3
CZMg_FMF_F2500	16.2	10.4 ± 0.4	75	0.508	27.1

[a]The theoretical composition of the precatalysts was in all cases Cu:Zn: Mg = 3.75:1.73:1.00. Experimentally found by ICP-OES for the TVT system was 3.74:1.61:1.00 and for the FMF [27] system 3.97:1.77:1.00.
[b]Calculated from the applied fluorine pressure used in each case.

metal hydroxide carbonate zincian malachite is clearly the main phase in both samples (see Figure 3A). However, the FMF sample also includes reflections clearly assigned to aurichalcite. This probably results from the different precipitation conditions. Shen et al. proved that the phase composition of the precipitation products in the synthesis of Cu/ZnO catalysts is dependent on the rate of addition of the solutions during the precipitation synthesis [33] because it influences the local concentration of the participating ions [33]. Since our coprecipitations necessarily used very different addition rates (FMF: 13 mL min^{-1} and TVT: 250 mL min^{-1}; Section 2.1 SI), the use of lower flow rates at FMF might also lead to the formation of aurichalcite as a secondary phase. Yet, the addition rate is only one parameter contributing to the precipitation conditions, and the local mixing conditions must be considered as well, but this exceeds the scope of this work.

IR spectra of the precursors include a characteristic carbonate double band, the position and intensity of which is almost identical in both samples (see Figure 3B). There is a difference in the OH band at ≈3350 cm^{-1}, where the TVT sample has a lower intensity and develops a splitting into two bands. In the fingerprint region (full IR spectra: SI, Section 3.3), clear similarities with crystalline malachite are evident, and the TVT sample has a somewhat higher intensity. A comparison of the TGA profiles of both samples shows that they are identical within the experimental error (see Figure 3C). With 144 $m^2\ g^{-1}$, the BET surface area of the CZMg_TVT_prec sample is a bit higher than that of the CZMg_FMF_prec sample with 124 $m^2\ g^{-1}$.

2.2.1.2 | Calcination. The subsequent calcination of both precursor samples provided the oxidic precatalysts. TVT and FMF samples were subjected to the identical calcination program at FMF (SI, Section 2.1), after which mainly CuO (tenorite) and ZnO (zincite) are visible as microcrystalline phases. The pXRD traces, IR spectra, TGA profiles, and BET surfaces of the precatalyst samples CZMg_TVT and CZMg_FMF are shown in Figure 3. When comparing the pXRD traces, two noticeable features can be observed:

1. The CZMg_TVT sample exhibits a significantly more intense zincian malachite reflection at 17.2° than the CZMg_FMF sample, which only shows a reflection with very low intensity.

2. In the CZMg_TVT sample, the reflections that can be assigned to ZnO are broader and less resolved than in the CZMg_FMF sample.

The IR spectra show carbonate bands of quite similar intensity, but the shoulder at 1638 cm^{-1} is more pronounced in the CZMg_FMF sample than in the TVT sample (Figure 3E). Analogously to the precursor samples, the OH band at around 3379 cm^{-1} is significantly less intense in the CZMg_TVT sample. A comparison of the TGA profiles of the two samples in Figure 3F shows no well-defined decomposition step for the FMF sample, but two clear decomposition steps for the TVT sample. This indicates that two types of carbonates are still present in the TVT material after calcination: "normal carbonates," which would normally be decomposed during calcination, and "high-temperature carbonates," which typically remain intact during calcination. One reason why "normal carbonates" are still contained in the TVT material may be the secondary particle size: while the sample precipitated at the FMF was dried *via* a spray drying process, the sample precipitated at the TVT was dried in a vacuum oven and then crushed as finely as possible in a mortar. However, this leads to significantly larger particles (10–300 µm) than the CZMg_FMF sample (1–5 µm). Due to the larger secondary particle size, carbonates can probably not be removed by calcination as efficiently as with smaller particle sizes, and a crystalline zincian malachite phase can still be observed after calcination (see below, SEM section).

The BET surface areas with respect to the precatalyst are reduced after calcination, and the BET surfaces of both precatalysts are now the same with 121 $m^2\ g^{-1}$ (cf. Figure 3D).

2.2.1.3 | SEM Data. In addition to the characterization methods discussed above, scanning electron microscope (SEM) data was obtained for the CZMg_TVT sample using the same

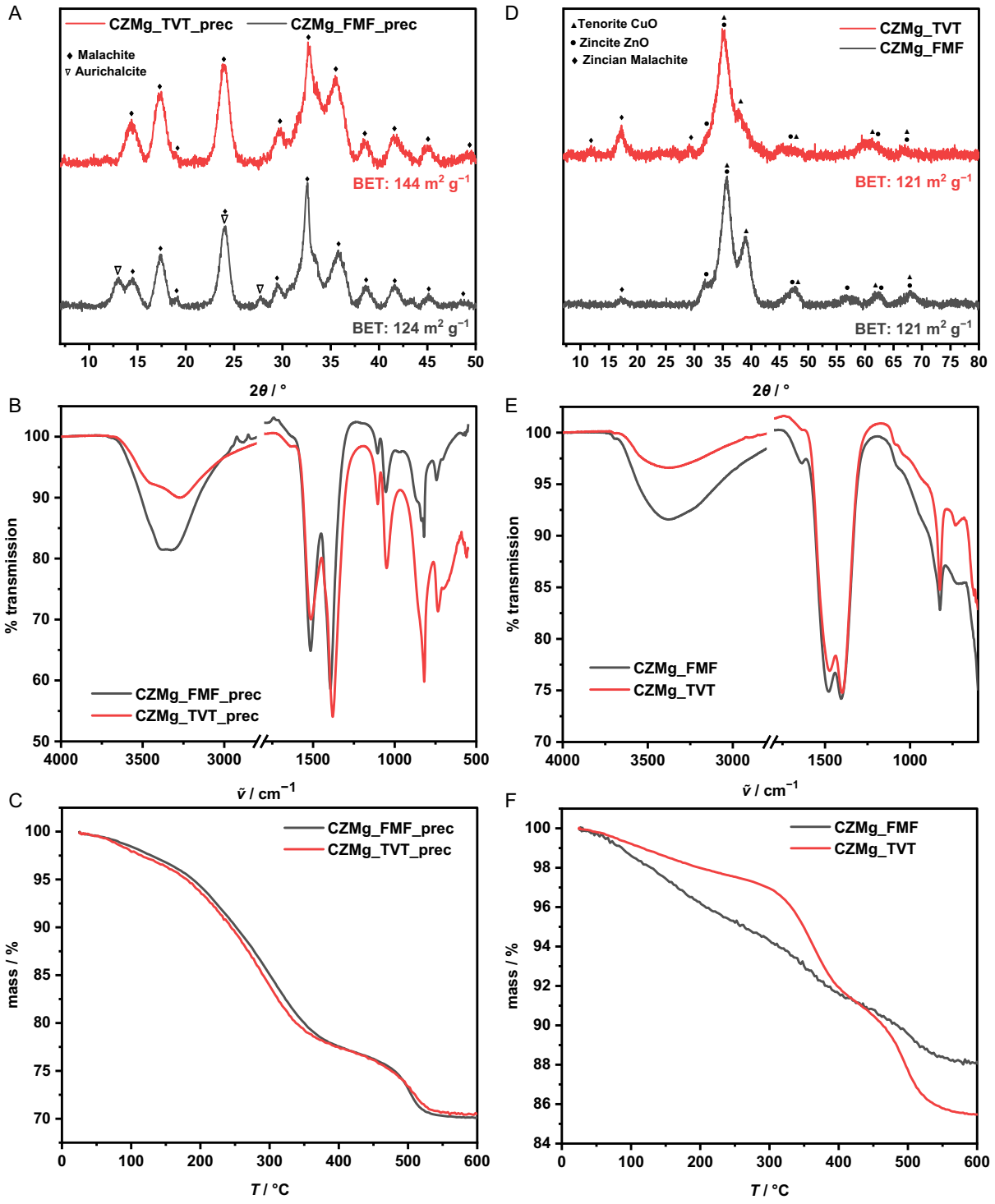

FIGURE 3 | Precursors (A–C) A: pXRD traces of the samples CZMg_TVT_prec and CZMg_FMF_prec, as well as phase assignment. For a more detailed phase assignment see SI Section 3. B: IR spectra of the two samples. C: TGA profiles of the two samples. Precatalysts (D–F): D: pXRD traces of the samples CZMg_TVT and CZMg_FMF, as well as phase assignment. For a more detailed phase assignment see SI Section 3. E: IR spectra of the two samples. F: TGA profiles of the two samples.

conditions and equipment than for CZMg_FMF (for the full data see section 3.7 SI). For both samples, a very fine and homogeneous microstructure is clearly recognizable at 50.000–250.000 magnification (Figure 4b–d,f–h). However, a comparison of the particle sizes between CZMg_TVT and CZMg_FMF at a magnification of only 2.000 (Figure 4a,e) shows an interesting difference: the CZMg_TVT sample has significantly larger particles (10–300 µm) than the CZMg_FMF sample (1–5 µm). Note that the secondary particles are visible here, but no conclusions can be drawn regarding the size of the corresponding primary particles. In contrast to the CZMg_FMF system, which obtains its small and homogeneously distributed particle size of the secondary particles through a spray-drying process, the CZMg_TVT system was crushed by grinding before calcination and has

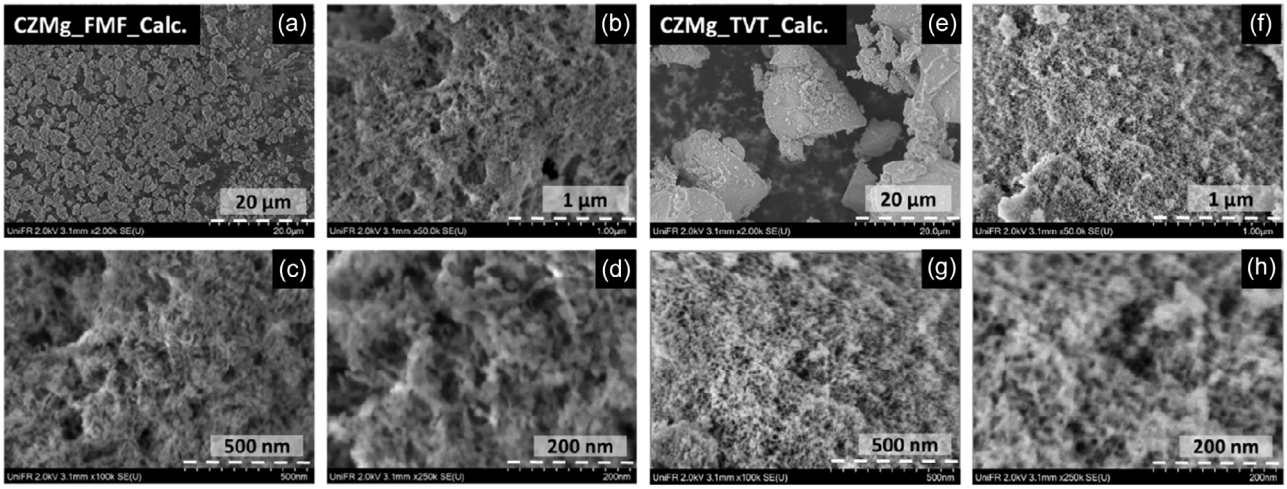

FIGURE 4 | SEM data of the samples CZMg_FMF (a–d) and CZMg_TVT (e–h) recorded with an acceleration voltage of 2 kV. Magnifications: 2000 (a,e), 50 000 (b,f), 100 000 (c,g), and 250 000 (d,h).

varying but larger secondary particle sizes caused by the grinding process. Yet, the higher resolution SEM pictures in Figure 4b–d,f-h indicate that the primary particle structure of the two materials is comparable. This agrees with all measurements described above.

2.2.2 | Oxidative Fluorination of the CZMg Precatalysts

Both precatalysts (CZMg_TVT and CZMg_FMF) were fluorinated by oxidative fluorination with F_2 to different degrees of fluorination. A comparison of the pXRD traces and a detail of the IR spectra of the precatalysts at different degrees of fluorination is shown in Figure 5.

Fluorination with a moderate amount of fluorine (F200) does not cause any noticeable changes in the pXRD trace. At higher degrees of fluorination, a reflex at 18.5° can be observed, which is most likely attributable to a Cu(OH)F phase (note that it is not trivial to distinguish between a Cu(OH)F phase and a $CuF_2{\cdot}2H_2O$ phase). This is in good agreement with conventionally precipitated CZMg catalysts [27, 29, 31]. The pXRD traces show that for both F1250 and F2500 precatalysts the sharp reflex assigned to Cu(OH)F is observed. Similar to before, the zincian malachite phase recognizable in CZMg_TVT (reflex at 17.2°) is also preserved at higher degrees of fluorination and the reflexes of the ZnO phase are also more pronounced in CZMg_FMF.

A comparison of the carbonate double bands in the IR spectra shows a notable difference between the two fluorination series: the CZMg_TVT series exhibits only a slight decrease in the intensity of the carbonate double band with increasing fluorination degree, whereas in the CZMg_FMF series a significantly stronger decrease in intensity, especially from F200 to F1250, is noted. This suggests that the amount of "high-temperature" carbonates that is still present after calcination has been reduced during fluorination more pronounced in the CZMg_FMF series.

The comparison of the TGA profiles of the two fluorination series in Figure 6 shows that the sample weights of the CZMg_TVT series after reaching 600°C have residual masses in a very narrow range (84.8%–85.5%), whereas the samples of the CZMg_FMF series have residual masses at 600°C found in a significantly wider range (88.2%–92.1%). The TGA profiles of the pristine precatalyst and the precatalyst with a low degree of fluorination (CZMg_TVT_F200) also show a clearly defined two-step stage, indicating that a significant number of "normal carbonates" is still present in the TVT material. In contrast, the profiles of the highly fluorinated TVT samples (F1250 and F2500) show only a single decomposition at around 300°C (onset), confirming the result already evidenced by IR spectroscopy that the highly fluorinated precatalysts have lost carbonates through the fluorination process, but more pronounced for the FMF series. The lower residual masses of the higher fluorinated TVT-series samples indicate a higher proportion of decomposable components than observed with the FMF series; these are most likely "high-temperature carbonates" that for morphological reasons (see SEM and Table 1) are more difficult to reach in the TVT system with large secondary particles and hence "survive" the F_2 treatment. These conclusions also agree with the surface area determinations of pristine and fluorinated precatalysts using N_2 physisorption (Table 1): They always show a reduction in the surface area from the precursor due to calcination. Fluorination leads only for CZMg_TVT_F200 to a small increase in SA_{BET} and in all other cases to a decrease with increasing fluoride content (F1250 and F2500).

This observation presumably stems from two opposing effects: (i) an increase in surface area due to oxidation-induced decomposition of carbonates ($CO_3^{2-} + F_2 \rightarrow CO_2 + 0.5\,O_2 + 2\,F^-$)—a 'chemical calcination'—and (ii) a reduction of the surface area caused by sintering processes, due to the high exothermicity of the fluorination reaction [31].

The higher BET surfaces of the TVT samples indicate slightly smaller primary particles, but as shown in Figure 4, the TVT samples have significantly larger secondary particle sizes. In addition, the pore volumes and median pore sizes of the FMF samples are all slightly larger than those of the TVT samples (Table 1; SI Section 3.4). Nevertheless, the TVT systems show higher measured fluoride contents than the FMF systems. This seemingly contradiction could be induced by the higher "normal carbonate" content of the nonfluorinated TVT sample. This allows the chemical calcination to take place to a greater extent during the fluorination process, in which F_2 converts these more accessible carbonate sites straight to CO_2 and O_2 gas ($CO_3^{2-} + F_2 \rightarrow CO_2 + ½\,O_2 + 2\,F^-$),

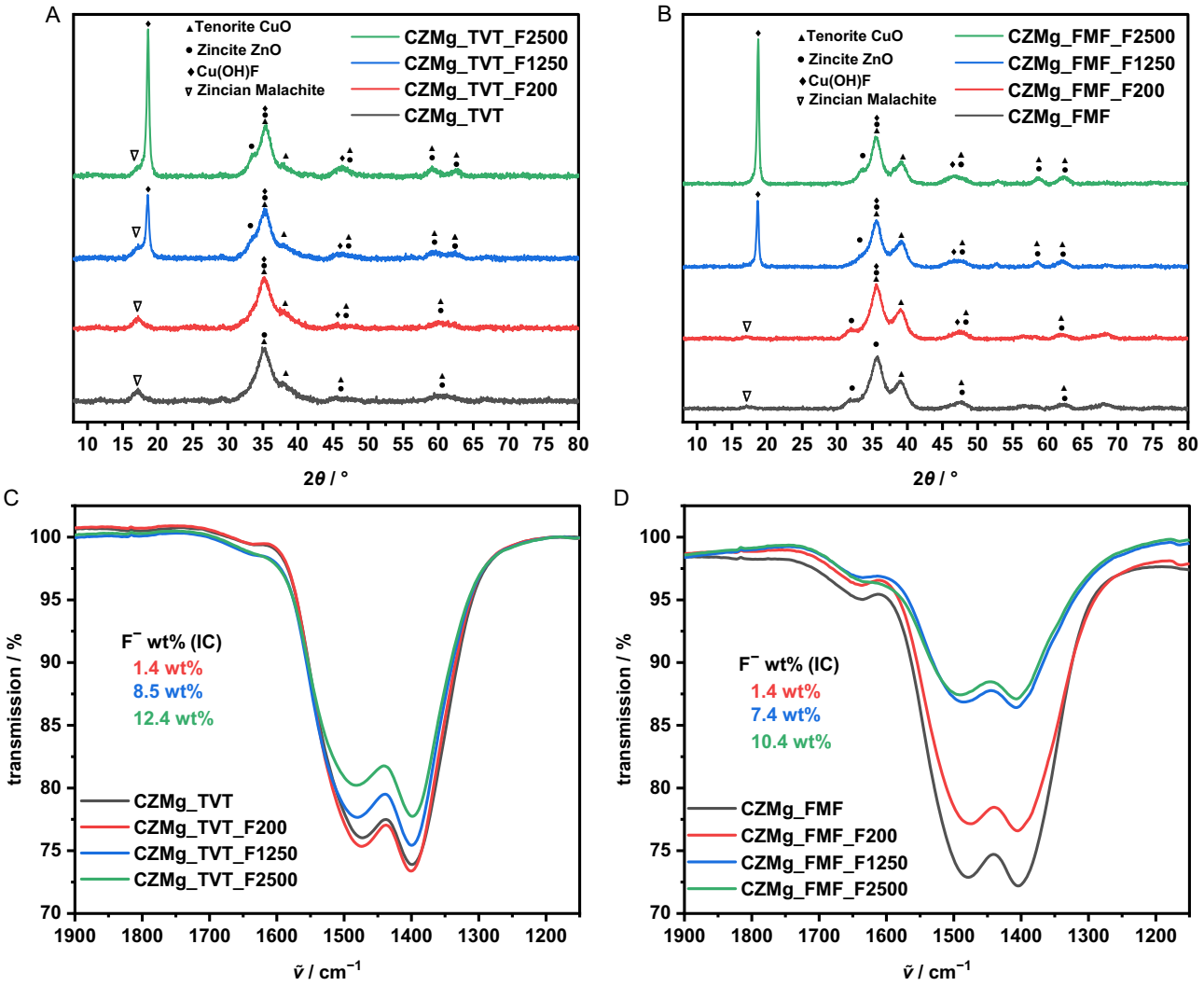

FIGURE 5 | (A) PXRD traces of the CZMg_TVT fluorination series. (B) PXRD traces of the CZMg_FMF fluorination series. (C) Detail of the IR spectra of the CZMg_TVT series showing the characteristic carbonate double band. (D) Detail of the IR spectra of the CZMg_FMF series showing the characteristic carbonate double band. All IR spectra were recorded under identical conditions: 64 scans, 4 cm^{-1}, ATR correction and background correction.

which rupture the structure of the particle and may lead to better fluorine uptake (F200 material). This also agrees with the consistently higher BET surfaces of the (fluorinated) TVT system class if compared to the FMF series: With less "normal carbonates" present in the FMF system and supported by larger total pore volume and median pore diameter in the FMF system (Table 1), the F_2 molecule has to penetrate (diffusion-limited) the core of the primary particles to also destroy part of the 'high-temperature' carbonates. Thus, in total, less carbonates are converted in the FMF system than the TVT system and a slightly lower fluoride content results with identical fluorination conditions and pressures (Table 1).

2.2.3 | Overview to the Standard Analytics Section

Using a jet mixer, a precursor is produced that, unlike the FMF precursor, contains only a crystalline zincian malachite phase and no aurichalcite phase. Additionally, the TVT precursor has a higher surface area than the FMF precursor. Subsequent calcination, carried out similarly for both samples, revealed further differences: the TVT sample exhibited a more intense reflection of the remaining zincian malachite phase, and the IR spectra and TGA profiles indicated a higher proportion of "normal carbonates." The FMF sample showed more intense reflections assignable to ZnO. The two precatalysts have the same BET surface area, and fluorination resulted in the formation of a Cu(OH)F phase in both samples at high fluoride content. However, unlike the CZMg_FMF fluorination series, the CZMg_TVT fluorination series exhibited a pXRD reflection assignable to zincian malachite at all degrees of fluorination. This agrees well with the analysis of the carbonate IR band intensity, which is influenced by fluorination to a much lesser extent in the CZMg-TVT system than in the CZMg-FMF system. Both fluorination series led to a decrease in BET surface area after fluorination, except for CZMg_TVT_F200. The FMF system tended to have lower surface areas but larger pore volumes and diameters than the TVT system. These differences are noticeable but rather small. These measurements and analyses provide evidence that both precatalyst materials are well-suited for the following investigation in catalytic reactions, as described in the succeeding section.

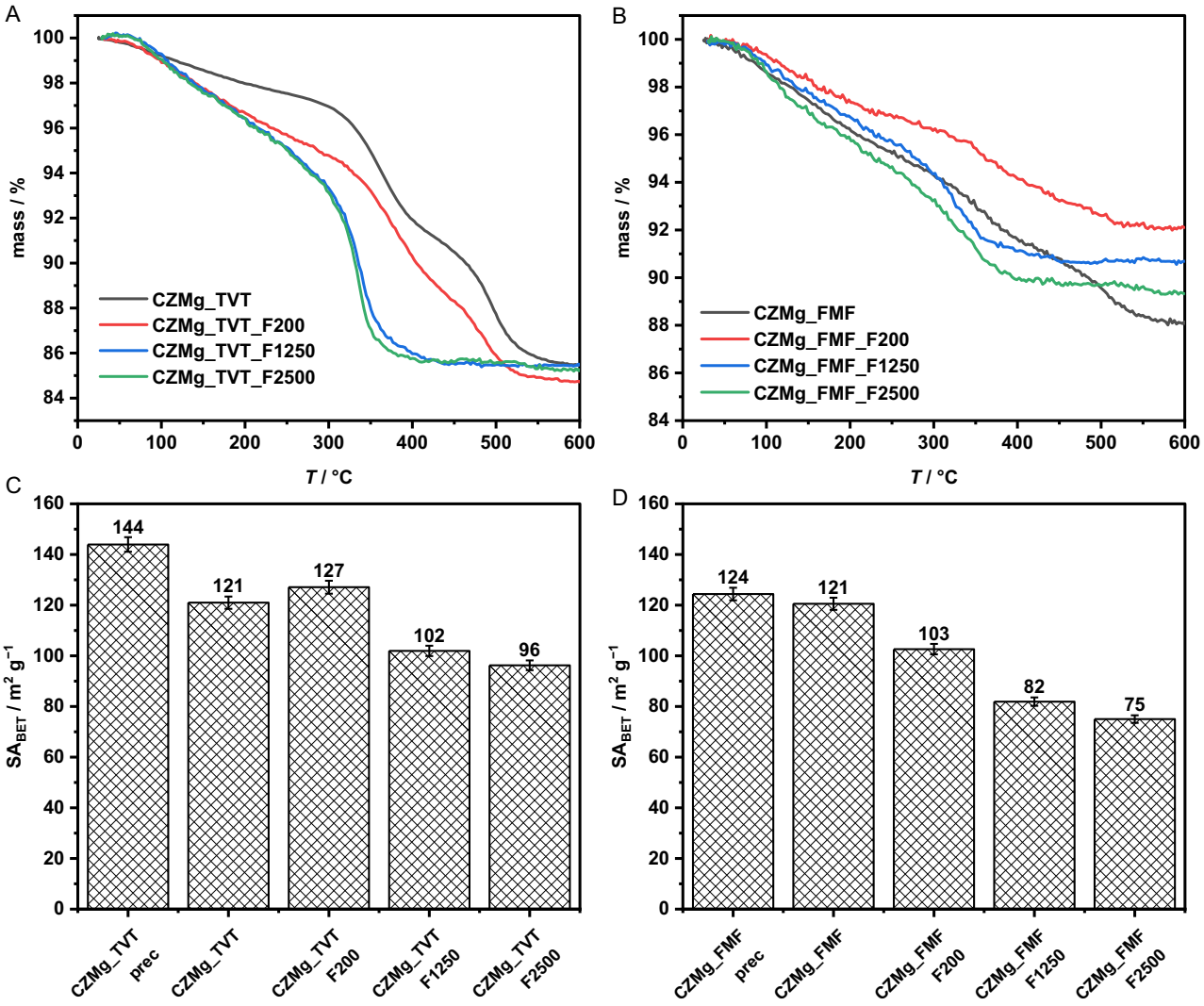

FIGURE 6 | (A) TGA profiles of the CZMg_TVT fluorination series. (B) TGA profiles of the CZMg_FMF fluorination series. (C) BET surface areas of the CZMg_TVT fluorination series. (C) BET surface areas of the CZMg_FMF fluorination series.

2.3 | Catalyst Measurements and Comparison of the TVT Systems with the FMF Systems

The fluorination series of the CZMg_FMF and CZMg_TVT systems were subjected to several catalysis measurements: a standard measurement (250°C, 40 bar, CO_2:H_2 = 1:3), a long-term measurement (time-on-stream TOS = 160 h), a measurement with varying CO_2/CO ratios (= CO_x variation measurement: $x = 1...2$) as well as a measurement in the kinetic regime and at different temperatures to determine the apparent activation energy for MeOH and CO formation. For the exact experimental details of the catalysis measurements, see SI Section 2.2.7.

2.3.1 | Standard Catalysis Measurements

The standard measurement for the CZMg_FMF series shows a maximum MeOH synthesis rate and MeOH selectivity for the CZMg_FMF_F200 system; the performance of the catalyst decreases as the degree of fluorination increases (Figure 7A). The CZMg_TVT series also shows a maximum MeOH synthesis productivity for the CZMg_TVT_F200 system (Figure 7B).

It is noticeable that all values for the MeOH and CO synthesis productivities of the CZMg_TVT series are a little bit better than the values of the CZMg_FMF series. Repeated measurements were used to determine the error of the setup used as at most 5%. Hence, the improvement observed is close to the error bars of our system. Still, each individual catalysis measurement was examined for its mass balance ($CO_{2,\ in}$ *vs.* sum of products + $CO_{2,\ out}$) to ensure correct data and agrees with the slight improvement of the TVT system.

2.3.2 | Catalysis Measurements over 160 H Time-on-Stream

In order to investigate the long-term stability of the systems produced, measurements were carried out with a TOS of 160 h (see Figure 8). This reveals a difference between the nonfluorinated systems CZMg_TVT and CZMg_FMF: The CZMg_TVT system is superior to the CZMg_FMF system in terms of MeOH synthesis rate and, in contrast to the CZMg_FMF system, has a higher MeOH synthesis rate in the first 50 h TOS and if compared to its fluorinated analogs. Towards the end of the 160 h TOS, the pristine CZMg_TVT system exhibits a comparable MeOH synthesis rate to its fluorinated analogs. This contrasts with the CZMg_FMF

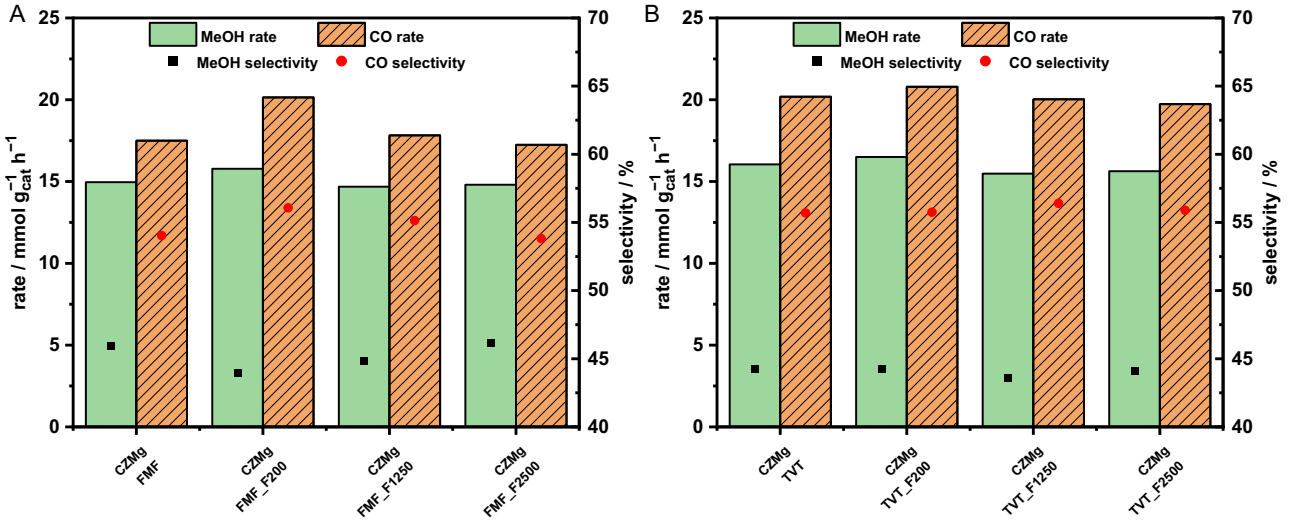

FIGURE 7 | Standard catalysis measurement (250°C, 40 bar, Gas Hourly Space Velocity (GHSV) = 19 800 NL kg$_{cat}^{-1}$ h^{-1}, CO_2:H_2 = 1:3, TOS = 45 h) of the CZMg_FMF series (A) and the CZMg_TVT series (B).

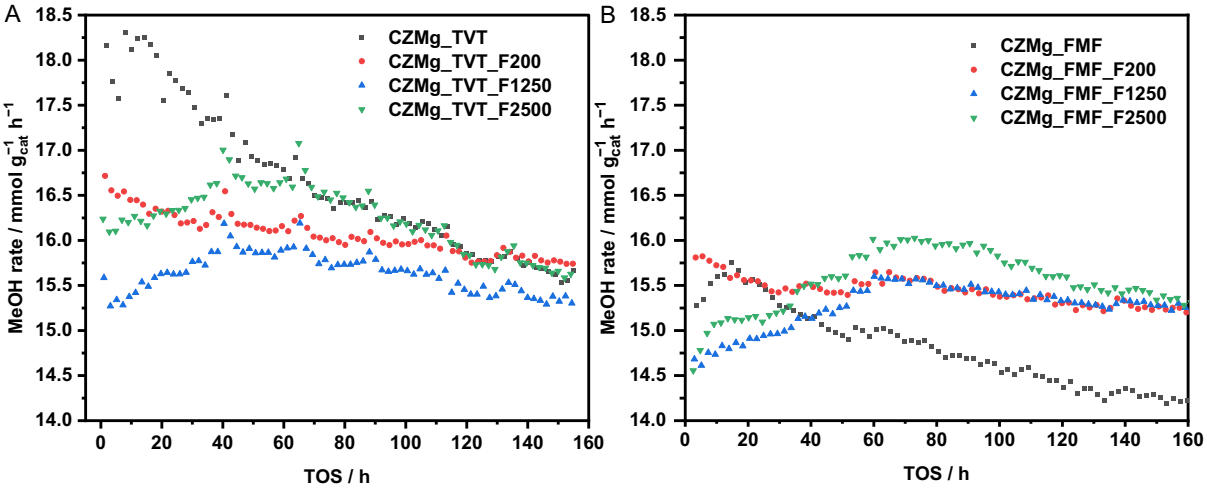

FIGURE 8 | Long-term catalysis measurement of CZMg_TVT_FXXX (250°C, 40 bar, GHSV 19 800 NL kg$_{cat}^{-1}$ h^{-1}, CO_2:H_2 = 1:3, TOS = 157 h) (A) and CZMg_FMF_FXXX (250°C, 40 bar, GHSV 19 800 NL kg$_{cat}^{-1}$ h^{-1}, CO_2:H_2 = 1:3, TOS = 160 h) (B).

series: here, the MeOH synthesis rate of the nonfluorinated system at the end of the measurement is lower than the synthesis rates of the fluorinated systems, which are all in a similar range. Yet, after 160 h TOS, the fluorinated CZMg_FMF systems and all CZMg_TVT systems converge to the, within the error bars, same methanol synthesis rate of 15.5 ± 0.3 mmol g$_{cat}^{-1}$ h^{-1}. In any case, oxidative fluorination realized after 160 h TOS a stabilization of the MeOH synthesis rate with respect to the pristine catalyst system: The deactivation slopes starting after the first induction phase of about 40–60 h are smaller for most fluorinated systems in comparison to their pristine CZMg analogs and would suggest a better long-term performance. The_F200 and _F1250 systems appear to be preferred from this perspective.

2.3.3 | Feed Gas Variation: Varying CO_x Content from $x = 1$ to 2

In order to investigate how these catalyst systems behave in CO/CO_2 feed gas mixtures, CO_x variation measurements were carried out in nine steps with x ranging from 1 to 2 (see Figure 9). Both fluorination series show the highest MeOH synthesis rates for all CO_x values for the F200 systems. In both series, only the nonfluorinated systems and the F200 systems form at integral conversion a typical volcano shape, which is caused by self-inhibition through the increased water amounts produced at higher CO_2 concentrations. Hence, at low CO_2 and H_2O concentrations, water also reacts with CO *via* the water gas shift reaction to generate additional H_2 and CO_2. The latter serves as the carbon source for MeOH formation [34]. With increased CO_2 concentrations, the stoichiometrically formed water binds strongly to the active sites, resulting in the blockage of the CO_2 hydrogenation sites [35, 36]. This leads to maximum of MeOH productivity at lower CO_2 levels. By contrast, for highly fluorinated catalysts (F1250, F2500), this maximum is suppressed, suggesting that fluorination suppresses WGS activity, which is known to occur at a different active site than MeOH synthesis.

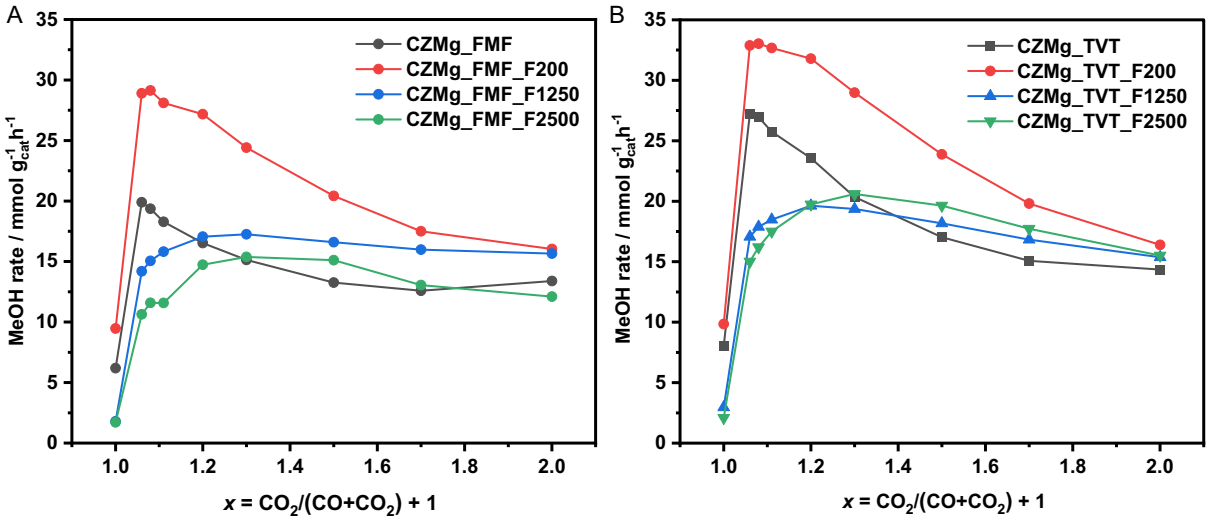

FIGURE 9 | CO_x variation measurement of the CZMg_FMF series (A) and the CZMg_TVT series (B). Measurement parameters: 250°C, CO_2: H_2 = 1:3, 40 bar, GHSV = 19 800 NL kg_{cat}^{-1} h^{-1}, TOS = 27 h. Direction of CO_x ratio change was from 2.0 to 1.0. For a description of the measurement protocol that kept the total flow rate identical see SI Section 2.2.7.

2.3.4 | Determination of the Apparent Activation Energies

In order to determine the apparent activation energies for the MeOH synthesis reaction ($E_{A,app,MeOH}$) and the CO synthesis reaction ($E_{A,app,CO}$) of the two catalyst series, measurements were carried out with high GHSV to ensure that the catalysts operate under differential conditions in the kinetic regime with CO_2 conversions < 5%. Hence, the MeOH and CO synthesis rates were determined by measuring the MeOH synthesis rate at 210°C, 220°C, 230°C, 240°C, and 250°C (total TOS = 24 h; SI 3.8.3). The apparent activation energies were calculated according to the Arrhenius equation. They are included in Table 2 and compared there with literature-known values.

The values for $E_{A,app,MeOH}$ of the CZMg_FMF series are slightly higher than the values of the TVT series at all degrees of fluorination. In both series, starting from the pristine system, the apparent activation energy decreases slightly due to fluorination, only to increase again at highest degrees of fluorination. The values for $E_{A,app,CO}$ show the same trend: For almost all systems of the FMF series, the apparent activation energy is higher than for the comparable systems of the TVT series. In both series, a maximum of $E_{A,app,CO}$ is found for the pristine system, thereafter $E_{A,app,CO}$ decreases with fluorination.

One reason for the slightly better performance of the TVT system could be the purer phase composition of the CZMg_TVT precursor, which includes zincian malachite as the only crystalline phase. This is known to be the best precursor phase for obtaining high-performance methanol synthesis catalysts [23, 26, 40, 41]. In contrast, the CZMg_FMF precursor sample showed the presence of an aurichalcite phase in addition to zincian malachite. Agreeing with this, the CO_x variation measurements of the two systems showed all values for the TVT series were slightly higher and that the apparent activation energies were the lowest in each comparable series, both for $E_{A,app,MeOH}$ and $E_{A,app,CO}$. Still, all of the apparent activation energies measured are in good agreement with those published earlier (cf. Table 2) [27–29, 31] while being in the lower range and indicative for a good catalyst system. Overall, no change in the active site of mechanism

TABLE 2 | Apparent activation energies calculated from measurements at high space velocity, low conversion, and different temperatures (see SI Section 3.8).

	$E_{A,app}$ (MeOH)/kJ mol^{-1}		$E_{A,app}$ (CO)/kJ mol^{-1}	
Catalyst Systems	**FMF [27]**	**TVT**	**FMF [27]**	**TVT**
CZMg	52 ± 2	45 ± 2	147 ± 4	132 ± 3
CZMg_F200	45 ± 2	42 ± 2	124 ± 2	125 ± 1
CZMg_F1250	43 ± 3	42 ± 2	123 ± 4	125 ± 5
CZMg_F2500	46 ± 2	45 ± 2	128 ± 4	123 ± 2
Literature	$E_{A,app}$ (MeOH)/kJ mol^{-1}		$E_{A,app}$ (CO)/kJ mol^{-1}	
CZZ [37]	41 ± 2		125 ± 3	
CZA [38]	57 ± 3		126 ± 1	
CZ [39]	57 ± 3		—	
CZ [28]	55 ± 3		130 ± 3	

[3, 4, 30] of MeOH or CO synthesis reactions is expected from the data collected here.

3 | Conclusion

The precipitation of the precursors in Karlsruhe (TVT) and in Freiburg (FMF) produced rather similar systems, which, however, have only one significant difference: The TVT precursor phase consists only of crystalline zincian malachite, whereas the FMF sample still has aurichalcite as a secondary phase. In addition, the size of the secondary particles of the FMF system is significantly smaller, while primary TVT particles were indirectly shown to be smaller, to have larger BET surfaces and smaller pore volumes and median pore diameters. These changes probably also account for further differences such as carbonate content and catalytic performance. Various catalysis measurements have shown that the TVT materials are slightly superior to the FMF system. Measurements of the apparent activation energies showed a tendency towards lower $E_{A,app}$ for MeOH formation and CO formation for all TVT systems compared to the FMF systems, which was reflected in higher synthesis rates in each case. The CZMg_TVT_F200 system shows exceptionally high activity in a feed gas with a high CO content. Fluorination of both CZMg catalyst systems to a low to medium degree (_F200 or _F1250) makes their performance more long-living, with smallest deactivation slopes of the stabilized MeOH synthesis rate starting after 40–60 h TOS.

Acknowledgments

L.D.E. thanks the Deutsche Bundesstiftung Umwelt (DBU) for a PhD scholarship. This work was supported by the University of Freiburg, the Freiburg Material Research Center (FMF) Team, and the Federal Ministry of Education and Research, BMBF (in the projects BioDME 02WER1528B, and NaMoSyn 03SF0566B0). The use of the SEM/EDX setup, acquired through the BMBF project EDELKAT (FKZ 03X5524), is gratefully acknowledged. We would like to thank A. Warmbold for help with the TGA and BET measurements, Dr. T. Ludwig for support regarding the powder X-ray diffraction, Carina Riecken and Svenja Kalthoff for help with the ICP-OES measurements and Dr. D. Kubas, Felix Hilfinger, and Henrik Schuster for many fruitful discussions.

Open Access funding enabled and organized by Projekt DEAL.

Conflicts of Interest

The authors declare no conflicts of interest.

References

1. F. Hong, Y. Qi, Z. Yang, et al., "Recent Advances in CO_2 Hydrogenation to Methanol," *DeCarbon* 8 (2025): 100111.

2. C. Jia, X. Tan, Q. Sun, et al., "Operando Identification of Active Sites in Cu-Based Catalysts for Efficient CO_2 Hydrogenation," *Advanced Materials* 37 (2025): e2417443.

3. A. Jurado, A. D., M. D. Higham, C. R. A. Catlow, and I. Krossing, "Fluorinated Copper Catalysts for Enhanced Methanol Synthesis from CO_2," *ChemCatChem*. (2025): e00824.

4. A. Jurado, A. D., M. D. Higham, Y. R. Poh, C. R. A. Catlow, and I. Krossing, "Structure–Activity Relationships of Fluorinated Cu-Based Catalysts for CO_2 Hydrogenation to Methanol," *Journal of Catalysis* 446 (2025): 115997.

5. S. Sajnani, M. A. Memon, S. A. Memon, et al., "Recent Advances in Catalysts for CO_2 Hydrogenation to Methanol: Design, Mechanism, and Performance," *Processes* 13 (2025): 314.

6. R. Salami, Y. Zeng, X. Han, S. Rohani, and Y. Zheng, "Recent Progress in Catalysts for CO_2 Hydrogenation to Methanol," *Journal of Energy Chemistry* 101 (2025): 345–384.

7. J. Ye, N. Dimitratos, L. M. Rossi, N. Thonemann, A. M. Beale, and R. Wojcieszak, "Catalysis for a Sustainable Future," *Science (new York, N.y.)* 387 (2025): eadn9388.

8. E. G. Aklilu and T. Bounahmidi, "Hydrogen Production and Utilization in Sustainable Energy Systems: A Review," *International Journal of Hydrogen Energy* 61 (2024): 578–602.

9. T. P. Araújo, S. Mitchell, and J. Pérez-Ramírez, "Advanced Catalytic Materials for Sustainable Chemical Processes," *Advanced Materials* 36 (2024): e2409322.

10. M. Corda, S. A. Chernyak, M. Marinova, et al., "Copper-Based Catalysts for Efficient CO_2 Hydrogenation to Methanol," *ACS Catalysis* 14 (2024): 17244–17255.

11. S. Hong, K. P. Reddy, Y. Song, D. Park, J. Y. Park, and J. Catal, "Surface Structure Effects on CO_2 Hydrogenation over Cu-Based Catalysts," *Journal of Catalysis* 437 (2024): 115643.

12. X. Liu, H. Zhang, J. Du, and J. Liao, "Process Safety Considerations in CO_2 Hydrogenation and Methanol Production," *Process Safety and Environmental Protection* 189 (2024): 1071–1086.

13. G. Pacchioni, "The Role of Surface Science in Heterogeneous Catalysis," *ACS Catalysis* 14 (2024): 2730–2745.

14. T. Pinheiro Araújo, G. Giannakakis, J. Morales-Vidal, et al., "Catalyst Design Strategies for CO_2 Hydrogenation," *Nature Communications* 15 (2024): 3101.

15. M. A. Tedeeva, A. L. Kustov, A. M. Batkin, et al., "Catalytic Conversion of CO_2 to Methanol over Modified Copper Catalysts," *Molecular Catalysis* 566 (2024): 114403.

16. W. Xiong, Z. Wu, X. Chen, et al., "Recent Advances in Copper-Based Catalysts for CO_2 Hydrogenation to Methanol," *Science China Chemistry* 67 (2024): 715–728.

17. W. Xiong, Z. Wu, X. Chen, et al., "Recent Advances in Copper-Based Catalysts for CO_2 Hydrogenation to Methanol," *Science China Chemistry* 67 (2024): 715–728.

18. A. Billion, A. Vogel, J. Schulte, H. Scherer, and I. Krossing, "Fluorinated Copper Catalysts for Improved Methanol Synthesis," *ChemCatChem* 15 (2023): e202300844.

19. D. Kordus, J. Jelic, M. Lopez Luna, et al., "Dynamic Restructuring of Copper Catalysts during CO_2 Hydrogenation," *Journal of the American Chemical Society* 145 (2023): 3016–3030.

20. M. Usman, M. D. Garba, Z. Zeb, et al., Catalytic Conversion of CO_2 into Methanol, *Sustainable Materials and Technology*, eds. M. Jawaid and A. Khan (Singapore: Springer Nature, 2023, pp. 37–59

21. L. Xu, X. Chen, C. Deng, et al., "Atmospheric CO_2 Reduction Strategies and Environmental Implications," *Atmosphere* 14 (2023): 1208.

22. M. Behrens, "The Active Site of Methanol Synthesis over Cu/ZnO Catalysts," *Catalysis Today* 246 (2015): 46–54.

23. M. Behrens, "Understanding the Catalytic Activity of Copper-Based Methanol Synthesis Catalysts," *Journal of Catalysis* 267 (2009): 24–29.

24. S. Zander, B. Seidlhofer, and M. Behrens, "Structural Evolution of Cu/ZnO Catalysts during Methanol Synthesis," *Dalton Transactions* 41 (2012): 13413–13420.

25. S. Kaluza, M. Behrens, N. Schiefenhövel, et al., "Influence of Catalyst Preparation on Cu/ZnO-Based Methanol Synthesis Catalysts," *ChemCatChem* 3 (2011): 189–199.

26. D. Guse, S. Polierer, S. Wild, S. Pitter, and M. Kind, "Process Optimization for Methanol Synthesis Catalysts," *Chemie Ingenieur Technik* 94 (2022): 314–327.

27. L. D. Ernst, L. Schmalenbach, S. Polinski, et al., "Advanced Fluorinated Catalysts for CO_2 Hydrogenation to Methanol," *ChemCatChem*. (2025): e01348.

28. V. Dybbert, S. M. Fehr, F. Klein, et al. "Highly Active Fluorinated Copper Catalysts for Methanol Synthesis," *Angewandte Chemie International Edition* 58 (2019): 12935–12939.

29. S. M. Fehr, K. Nguyen, C. Njel, and I. Krossing, "Fluorination Effects in Copper-Based Catalysts for Methanol Synthesis," *ACS Catalysis* 11 (2021): 13223–13235.

30. S. M. Fehr, K. Nguyen, and I. Krossing, *Fluorinated Catalyst Systems for Efficient Methanol Production* (ChemCatChem 2022). 14

31. L. D. Ernst, C. Njel, W. Marquart, et al., "Oxidative Fluorination of a Ternary Cu/ZnO/FeO_x Methanol Catalyst—A Proof of Principle," *ACS Catalysis* 14 (2024): 12199–12213.

32. E. Frei, A. Schaadt, T. Ludwig, H. Hillebrecht, and I. Krossing, "Synthesis and Characterization of Fluorinated Copper Oxide Materials for Catalytic Applications," *ChemCatChem* 6 (2014): 1721–1730.

33. G. Shen, "Structure Sensitivity of Methanol Synthesis over Copper-Based Catalysts," *Journal of Catalysis* 138 (1992): 754–763.

34. M. Sahibzada, I. S. Metcalfe, and D. Chadwick, "Methanol Synthesis from CO_2/CO/H_2 over Cu/ZnO-Based Catalysts," *Journal of Catalysis* 174 (1998): 111–118.

35. J. S. Lee, K. H. Lee, S. Y. Lee, and Y. G. Kim, "Kinetic Study of Methanol Synthesis over Cu/ZnO/Al_2O_3 Catalysts," *Journal of Catalysis* 144 (1993): 414–424.

36. G. Liu, D. Willcox, M. Garland, and H. H. Kung, "Kinetics of Methanol Synthesis over Copper-Based Catalysts," *Journal of Catalysis* 90 (1984): 139–149.

37. D. Kubas, M. Semmel, O. Salem, and I. Krossing, "Fluorinated Copper-Based Catalysts for Methanol Synthesis," *ACS Catalysis* 13 (2023): 3960–3972.

38. J. Schumann, T. Lunkenbein, A. Tarasov, N. Thomas, R. Schlögl, and M. Behrens, "Structure–Activity Relationships in Cu/ZnO Catalysts for Methanol Synthesis," *ChemCatChem* 6 (2014): 2889–2897.

39. F. Studt, M. Behrens, E. L. Kunkes, et al., "The Mechanism of CO and CO_2 Hydrogenation to Methanol over Cu-Based Catalysts," *ChemCatChem* 7 (2015): 1105–1111.

40. D. Waller, D. Stirling, F. S. Stone, and M. S. Spencer, "The Activity of Copper/Zinc Oxide Catalysts for Methanol Synthesis," *Faraday Discussions of the Chemical Society* 87 (1989): 107–120.

41. M. Behrens and F. Girgsdies, "Structural Analysis of Copper/Zinc Oxide Catalysts for Methanol Synthesis," *Zeitschrift für Anorganische Und Allgemeine Chemie* 636 (2010): 919–927.

Supporting Information

Additional supporting information can be found online in the Supporting Information section.